Millimeter emission from protoplanetary disks : dust, cold gas, and relativistic electrons

Salter, D.M.

Chapter 6

Hunting for Millimeter Flares from Magnetic Reconnection in Pre-main-sequence Spectroscopic Binaries

Recent observations of the low-mass pre-main-sequence (PMS), eccentric spectroscopic binaries DQ Tau and V773 Tau A reveal that their millimeter spectrum is occasionally dominated by flares from non-thermal emission processes. The transient activity is believed to be synchrotron in nature, resulting from powerful magnetic reconnection events when the separate magnetic structures of the binary components are briefly capable of interacting and forced to reorganize, typically near periastron. We conducted the first systematic study of the millimeter variability toward a sample of 12 PMS spectroscopic binaries with the aim to characterize the proliferation of flares amongst sources likely to experience interbinary reconnection events. The source sample consists entirely of short-period, close-separation binaries that possess either a high orbital eccentricity ($e > 0.1$) or a circular orbit ($e \approx 0$). Using the MAMBO2 array on the IRAM 30m telescope, we carried out continuous monitoring at 1.25 mm (240 GHz) over a 4-night period during which all of the high-eccentricity binaries approached periastron. We also obtained simultaneous optical VRI measurements, since a strong link is often observed between stellar reconnection events (traced via X-rays) and optical brightenings. UZ Tau E is the only source to be detected at millimeter wavelengths, and it exhibited significant variation ($F_{1.25\mathrm{mm}} = 87$–179 mJy); it is also the only source to undergo strong simultaneous optical variability ($\Delta R \approx 0.9$ mag). The binary possesses the largest orbital eccentricity in the current sample, a predicted factor in star-star magnetic interaction events. With orbital parameters and variable accretion activity similar to DQ Tau, the millimeter behavior of UZ Tau E draws many parallels to the DQ Tau model for colliding magnetospheres. However, on the basis of our observations alone, we cannot determine whether the variability is repetitive, or if it is due to variable free-free emission in an ionized wind. UZ Tau E brings the number of known millimeter-varying PMS sources to 3 out of a total of 14 monitored binaries now in the literature. We favor a model whereby repeated magnetospheric interactions near closest approach are responsible for the millimeter-wave variability of UZ Tau E, analogous to the model for DQ Tau. However, given the small number statistics, we cannot exclude powerful interbinary reconnection events as a rare, stochastic phenomenon.

Á. Kóspál, D. M. Salter, M. R. Hogerheijde, A. Moór, and G. A. Blake
Astronomy & Astrophysics, submitted (2010)

6.1 Introduction

Recent observations of young stellar objects (YSOs) are challenging the long-standing notion that the millimeter continuum emission characterizing these objects is always dominated by the quiescent thermal emission from passively-heated circumstellar dust. Powerful, transient millimeter flares attributed to synchrotron continua have now been reported toward two embedded protostars in the Corona Australis cloud (Choi et al. 2009), one protostar in the Orion BN/KL star-forming region (Forbrich et al. 2008), the embedded YSO GMR-A in Orion (Bower et al. 2003; Furuya et al. 2003), the classical T Tauri star (CTTS) DQ Tau in Taurus (Chapters 4 and 5, Salter et al. 2008, 2010), and the weak-line T Tauri star (WTTS) V773 Tau A, also in Taurus (Massi et al. 2002, 2006, 2008).

These millimeter flares are thought to be more powerful examples of the prevalent, lower-energy radio activity observed toward YSOs, and are not unlike flares accurring on the Sun (Stine et al. 1988; White et al. 1992). The emission is attributed to a combination of gyrosynchrotron and synchrotron radiation powered by magnetic reconnection events in the stellar coronae, which occur when oppositely directed magnetic field lines interact (Bastian et al. 1998). The radio flare resulting from this magnetic activity is also expected to be accompanied by an X-ray flare of proportional luminosty according to the Neupert effect (Neupert 1968; Güdel 2002). In this way, large X-ray surveys are contributing to the characterization of the magnetic activity during the T Tauri phase (e.g. Getman et al. 2005; Güdel et al. 2007), which represents the period during the formation and main sequence life of a solar-type star when magnetic activity levels are highest and when reconnection—and not accretion—is believed to be the primary X-ray production mechanism (Preibisch et al. 2005; Stassun et al. 2006, 2007; Forbrich et al. 2007; Feigelson et al. 2007). The X-ray data confirm analogous solar-type coronal activity, but with luminosities 10^3–10^5 times higher (Testa 2010). Uninterrupted, long-duration observing campaigns of star-forming regions also document a once-a-week statistical occurrence of giant X-ray flares, representing the most powerful events and an estimated 1% of all flares (Favata et al. 2005; Getman et al. 2008a,b). If magnetic activity is indeed the trigger, then these X-ray events are most likely to be associated with synchrotron emission processes extending into the millimeter regime.

It is noteworthy that in the two best-studied millimeter flare cases, both DQ Tau and V773 Tau A are close-separation, eccentric, pre-main-sequence (PMS) binaries with similar orbital characteristics. In addition, their flaring was recurring, leading the authors in the latest study to conclude that DQ Tau could display excess millimeter flux as much as 8% of the time, with consistency near periastron. One can thus speculate that in close binaries, in addition to the single-star coronal activity described until now, two additional magnetic activity scenarios might exist. An example of the first is V773 Tau A, where interbinary interactions due to chance alignments of narrow extended coronal features, like helmet streamers, cause the flares. The second binary-specific phenomenon is the current model for DQ Tau where colliding dipolar magnetospheres represent a simple geometric scenario for periodic events, with two primary determining factors: a periastron approach smaller than twice the magnetospheric radius ($R \sim 5\,R_\star$) and a high eccentricity. In this arrangement, the closed stellar magnetospheres must overlap near periastron, but only temporarily.

Again, X-ray studies can provide constraints on the coronal extent of PMS stars, with the result that typical inferred loop lengths are 4–20 $R_\star$ for the most powerful outbursts. This is much larger than any coronal structure observed toward more evolved stars (Favata et al. 2005), and consistent with the T Tauri stage being the most magnetically active phase of star formation. In the case of the WTTS binary system V773 Tau A, two separate coronal structures extending to $\geq 15\,R_\star$ each are necessary to bridge the interbinary gap (Massi et al. 2008). Toward DQ Tau the derived loop lengths from both X-ray and millimeter analyses are $5\,R_\star$ in height (Getman et al. 2010, submitted; Chapter 4, Salter et al. 2010). If the X-ray statistics predict correctly a common once-a-week occurrence with consistently large loop lengths, then more interbinary collisions might be expected in a number of close-separation binaries, in

addition to any single-star events that may occur. Binary systems also occur frequently, representing 65% or more of the local field population in the middle of the main-sequence (Duquennoy & Mayor 1991). The fraction increases to up to 75% for the population in the Taurus star-forming region (Leinert et al. 1993; Ghez et al. 1997; Kohler & Leinert 1998; Luhman et al. 2010), suggesting that more systems could start out as binaries. Thus, candidate millimeter-variable systems are worthy of investigation.

To assess the proliferation of significant millimeter variability among PMS binaries, we report here on a targeted millimeter variability survey of 12 PMS spectroscopic binaries that are most likely to experience millimeter flares, based on predictions by the current interbinary magnetic reconnection models, either following the V773 Tau A scenario and exhibiting strong flares at many orbital phases, or exhibiting the DQ Tau phenomena showing flares with more regularity around periastron. Since in both the DQ Tau and UZ Tau E cases, optical brightenings are common near periastron due to periodic accretion events (Jensen et al. 2007), and because the optical light curve of DQ Tau was found to mirror its millimeter flare activity in both time and duration (Chapter 5, Salter et al. 2010), we complemented our millimeter data with simultaneous optical monitoring of our targets.

6.2 Observations

6.2.1 Target Selection

The study of PMS binaries is a relatively young field, due in large part to the difficult and time-consuming nature of spectroscopic observations, while sometimes further impeded by a complicated circumstellar environment. To date, orbital parameters have been published for only a few dozen young spectroscopic binaries. These parameters include the *necessary* selection criteria for the present study: known eccentricity (e), orbital period (P), projected semimajor axis ($a \sin i$), and the epoch of periastron passage. From the available sources in the literature, we selected objects that are observable from the northern hemisphere (located primarily in Taurus and Orion), and that possess an orbital period of less than 50 days. The latter constraint means that the periastron distances for these objects are in the range where magnetospheric or coronal interactions have occurred in similar systems. In addition, shorter periods make it easier to observe large numbers of binaries as they complete periastron passage around the same time.

The resulting list of targets, along with their most important orbital parameters, can be found in Table 6.1. Our sample is comprised of two separate groups. In the first group, we specifically target short-period binaries of high orbital eccentricity ($e > 0.1$) and small periastron separations similar to DQ Tau and V773 Tau A. In this half of the sample, the binary components are suspected to undergo a change in their large-scale magnetospheric topology as the binary separation distance varies greatly and rapidly near periastron. This group is most likely to experience a merging of the two magnetospheres near closest approach with a subsequent detachment at larger separations—much like the current picture for DQ Tau (Chapter 5, Salter et al. 2010). Although we note that none of the targets quite approach the exceptional combination of large eccentricity and close approach as DQ Tau (with its $e = 0.556$ and $d_{\rm min} = 13\,R_\odot$). The second group serves as a "control sample" and includes close-separation binaries with circular orbits ($e \approx 0$). Since the binary separation in these systems remains constant, there is no variable compression or relaxation of the component magnetospheres throughout the orbit, and therefore the global magnetospheric topology is relatively unchanged; reconnection is not expected to occur except sporadically in chance collisions of extended coronal features due to the stars' close proximity—similar to the current model for V773 Tau A (Massi et al. 2008).

6.2.2 Observations and Data Reduction

Millimeter Observations

We obtained millimeter data with the IRAM 30 m telescope on Pico Veleta (Spain) between 17–21 November 2009. We used the 117-pixel Max-Planck Millimeter Bolometer array (MAMBO2) in the standard ON/OFF mode, using a 35″ wobbler throw, and making sure that the target fell on the most sensitive pixel (pixel #20) during each on-source exposure. One scan consisted of four (on the first night) or eight (on the remaining three nights) subscans of 60 s exposure time. The MAMBO2 bandpass was centered at $\lambda = 1.25$ mm ($\nu = 240$ GHz). At this wavelength, the half power beamwidth is 11″ and the pixel spacing is 20″.

We monitored our targets for four consecutive nights, covering also the periastron events for most of the high-eccentricity binaries. We observed each target 1–3 times per night depending on weather conditions. The atmospheric transmission at 1.25 mm was usually good, with the zenith atmospheric opacity being monitored with sky dips every 1–2 hours. Opacity was consistently found to be between 0.1–0.4, except for a few peaks on the night of November 19/20. Sky noise levels were typically very low, except again for a few hours on the night of November 19/20. Mars and Uranus were used for focusing and gain calibration every 3–4 hours. Pointing was checked every 1–2 hours using Mars, Uranus, or a nearby quasar. Occasionally, high wind velocities during our observing run resulted in a lower pointing

Table 6.1 — Orbital parameters for the binaries.

Name	D [pc]	e	P [days]	$a \sin i$ [AU]	i [°]	$d_{\rm min}$ [$R_\odot$]	Ref.
High-eccentricity binaries							
EK Cep	164	0.109	4.43	0.077	89.3*	14.7	1,2
UZ Tau E	140	0.33	19.13	0.124	54	22.1	3
RX J0530.7−0434	460	0.32	40.57	0.336	78.5	>49.1	4,5
Parenago 1540	470	0.12	33.73	0.188	···	>35.6	6
Parenago 2494	470	0.257	19.48	0.146	···	>23.3	7
GG Ori	438	0.222	6.63	0.116	89.2*	19.4	8
Circular binaries							
RX J0350.5−1355	450**	0	9.28	0.115	···	>24.7	4
V826 Tau	150	0	3.89	0.013	13	12.6	9
RX J0529.4+0041	325	0	3.04	0.053	86.5*	11.5	10
Parenago 1802	420	0.029	4.67	0.050	78.1*	10.7	11
RX J0541.4−0324	450**	0	4.99	0.074	···	>15.9	4
NGC 2264 Walk 134	913	0	6.35	0.099	<73	>21.3	12,13
Binaries already known to exhibit flares							
DQ Tau	140	0.556	15.80	0.053	23	12.9	14
V773 Tau A	148.4	0.272	51.10	0.35	66.0	60.0	15

Notes. e is eccentricity; P is orbital period; a is semimajor axis; i is inclination; $d_{\rm min}$ is separation during periastron (or a lower limit for systems with an unknown inclination); * indicates eclipsing binaries; ** means the average distance to Orion was used. **References.** (1) Gimenez & Margrave (1985); (2) Torres et al. (2010); (3) Jensen et al. (2007); (4) Covino et al. (2001); (5) Marilli et al. (2007); (6) Marschall & Mathieu (1988); (7) Reipurth et al. (2002); (8) Torres et al. (2000); (9) Reipurth et al. (1990); (10) (Covino et al. 2004); (11) Stassun et al. (2008); (12) Padgett & Stapelfeldt (1994); (13) Baxter et al. (2009); (14) Mathieu et al. (1997); (15) Boden et al. (2007).

precision for some of the scans. As a result, we have determined that the absolute flux calibration for all data points is accurate to within ∼20%.

The data were reduced using the MOPSIC pipeline (developed by R. Zylka), and included steps to remove the atmospheric emission (using the two wobbler offset positions), to correct for extinction due to atmospheric water vapor (using the skydips), to perform gain calibration (using the calibration observations of bright sources with known 1.25 mm flux), and to calculate a noise-weighted average of the subscans. The obtained flux densities usually have a root mean square noise of 2–3 mJy bm^{-1}, and are listed per source in Table A.1.

Optical Observations

Simultaneous optical monitoring of our targets was conducted from two telescopes: the 60/90/180 cm (aperture diameter/primary mirror diameter/focal length) Schmidt telescope of the Konkoly Observatory (Hungary), and the 80 cm (primary mirror diameter) IAC-80 telescope of the Teide Observatory in the Canary Islands (Spain). The Konkoly Schmidt telescope is equipped with a 1536 × 1024 pixel Photometrics AT 200 CCD camera (pixel scale: 1.03″), and a Bessel UBV(RI)$_C$ filter set. The Teide IAC-80 telescope is equipped with a 2048 × 2048 pixel Spectral Instruments E2V 42-40 back-illuminated CCD camera 'CAMELOT' (pixel scale: 0.304″), and a Johnson-Bessel UBV(RI)$_J$ filter set. Images with the Schmidt telescope were obtained on 9 nights in the period between 13–26 November 2009, and with the IAC-80 telescope for 3 nights between 18–22 November 2009. With the IAC-80, only R-band images were taken, whereas with the Schmidt, R and I, and additionally for the brighter stars, V, images were also obtained. One of our targets, UZ Tau E, was observed with the IAC-80 telescope using VRI filters also between 25 October and 7 November 2009.

The images were reduced in IDL following the standard processing steps of bias subtraction, dark subtraction (for the Photometrics camera on the Schmidt telescope only) and flat-fielding. On each night, for each target, images were obtained in blocks of 3 or 5 frames per filter. Aperture photometry for the target and other field stars were performed on each image using IDL's *cntrd* and *aper* procedures. For the Schmidt images, we used a 5-pixel radius aperture, and a sky annulus between 10 and 15 pixels. For the IAC-80 images, the aperture radius was 8 pixels, and the sky annulus was between 30 and 40 pixels. In the case of RX J0529.4+0041, a hierarchical triple system, the spectroscopic binary and the tertiary component were partially resolved, so we increased the Schmidt aperture to 10 pixels and the IAC-80 aperture to 30 pixels, in order to make sure that the aperture included the total flux from all three components. In the case of UZ Tau, a hierarchical quadruple system, we obtained separate photometry for UZ Tau E and UZ Tau W in the following way. The small pixel scale and the good seeing at the IAC-80 telescope made it possible to obtain separate photometry for both the E and the W components, by using an aperture radius of 4 pixels. The results indicated that the W component was constant within 0.02 mag. For the Schmidt images, we used an aperture radius of 10 pixels (encompassing both UZ Tau E and W), and we subtracted the contribution of the W component (calculated as the average magnitude measured on the IAC-80 images).

For the purpose of differential photometry, we selected a comparison star for each of our targets. Our main selection criterium for the comparison stars was constant brightness during our observing period (compared to other stars in the field). The selected comparison stars are listed in Table A.2. We calculated the magnitude difference between our target and the comparison stars for each frame. Then, these differential magnitudes were averaged for each night, while their standard deviation was quadratically added to the formal photometric uncertainty. Due to the different filter sets on the two telescopes, the resulting magnitudes were slightly different, especially in cases where the comparison star was much redder than the target star. In these cases, we shifted the IAC-80 magnitudes by 0.03–0.08 mag so that they overlap with the Schmidt magnitudes obtained on the same nights. The resulting

(shifted) values can be found in Table A.3, and the light curves for the R filter are plotted in the top panels of Figure 6.1. The light curves for the other filters look very similar, but often have fewer available data points.

6.3 Results

In Figure 6.1 we show the optical and millimeter light curves for all of our targets, as well as the separation distances between the binary components, as a function of time. The optical light curves indicate that most of our targets showed variability at a certain level throughout our observing campaign. By far the highest amplitude in our sample was displayed by UZ Tau E, (with $\Delta R \approx 0.9$ mag), but NGC 2264 Walk 134 ($\Delta R \approx 0.2$ mag), and GG Ori ($\Delta R \approx 0.3$ mag) also varied significantly. The rest of the sample were either constant (EK Cep, RX J0529+0041), or showed slight variations of <0.1 mag. While UZ Tau E and NGC 2266 Walk 134 show variability on a daily timescale, the light curve for GG Ori exhibits only one dip, corresponding to an eclipse shortly before periastron. The sparsely-sampled optical light curves do not display any obvious periodicities in their own right, even with the broader optical monitoring period of 12-14 days and covering multiple orbital periods for some sources. However, in many cases the shapes and amplitudes may be consistent with rotational modulation of the light curve due to stellar spots (RX J0530.7−0434, Parenago 1540, Parenago 2494, RX J0350.5−1355, V826 Tau, Parenago 1802, and RX J0541.4−0324). Thus, a brightening of an eccentric source during periastron may be a chance coincidence. A more detailed analysis of the optical data on a source-by-source basis is given in Section 6.4.3.

At millimeter wavelengths, only one of our targets, UZ Tau, was detected. The other sources remained undetected with typical 3σ upper limits between 4 and 11 mJy. Apparently, UZ Tau is the only

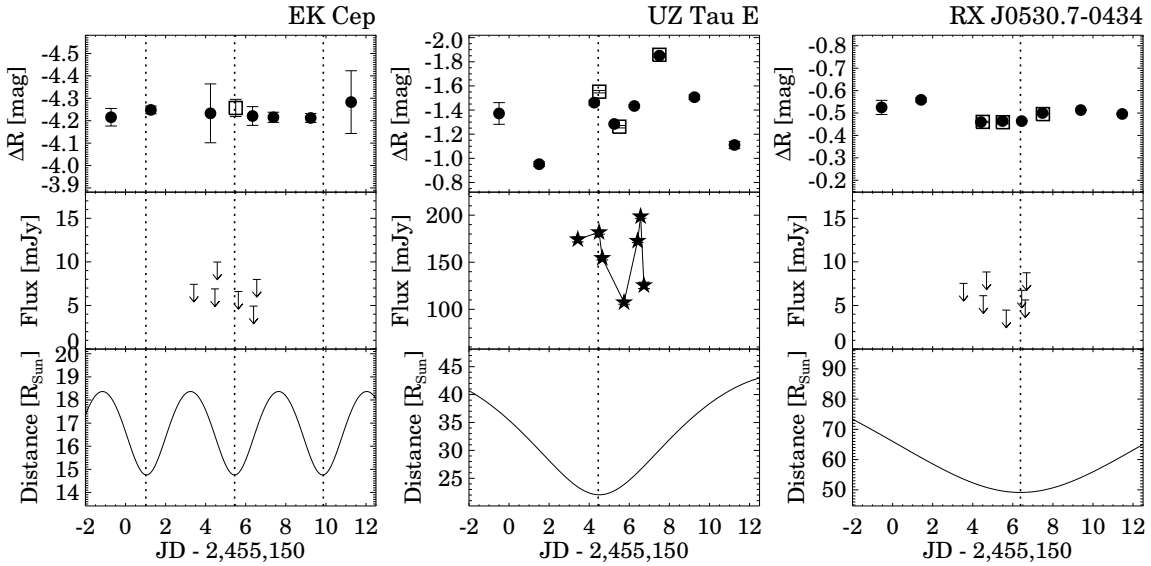

Figure 6.1 — Optical (top) and millimeter (middle) light curves for each of the spectroscopic binaries, as well as separation distances for the binary components as a function of time (bottom). *Filled dots:* R_C-band observations from the Konkoly Schmidt telescope in Hungary; *Open squares:* R_J-band observations from the Teide IAC-80 telescope in Spain; *Filled asterisks:* 1.25 mm observations with the IRAM 30 m telescope in Spain; *Arrows:* 3σ upper limits for the 1.25 mm fluxes. Note that the millimeter fluxes of UZ Tau E contain an $\approx$20 mJy contribution from UZ Tau W. For the high-eccentricity binaries, a vertical line indicates the time of periastron, while for the circular binaries, thick horizonal lines indicate the length of the orbit.

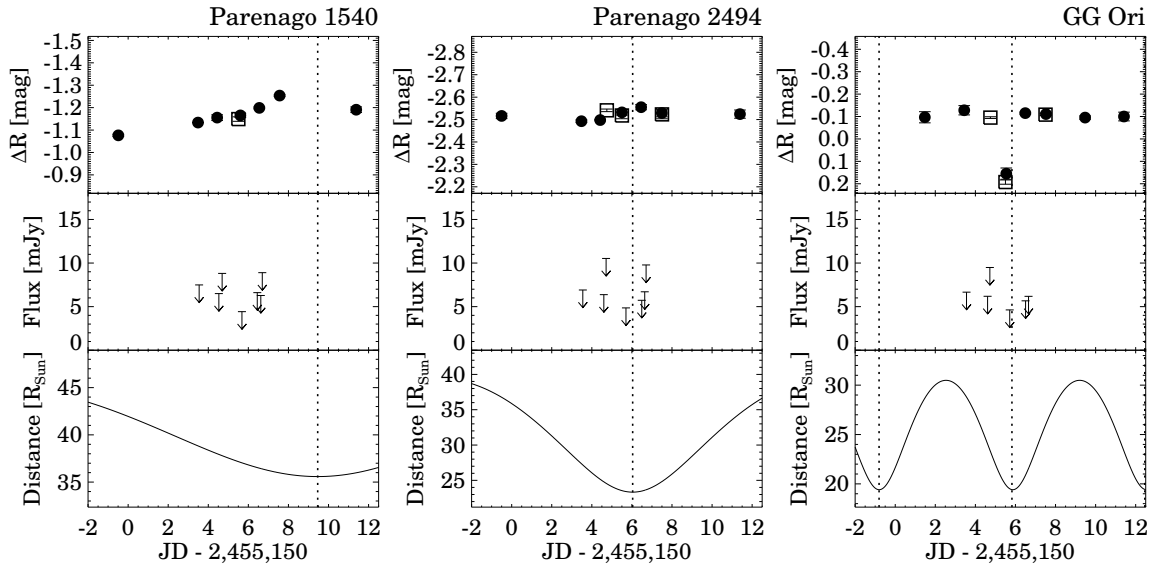

Figure 6.1 — (Continued)

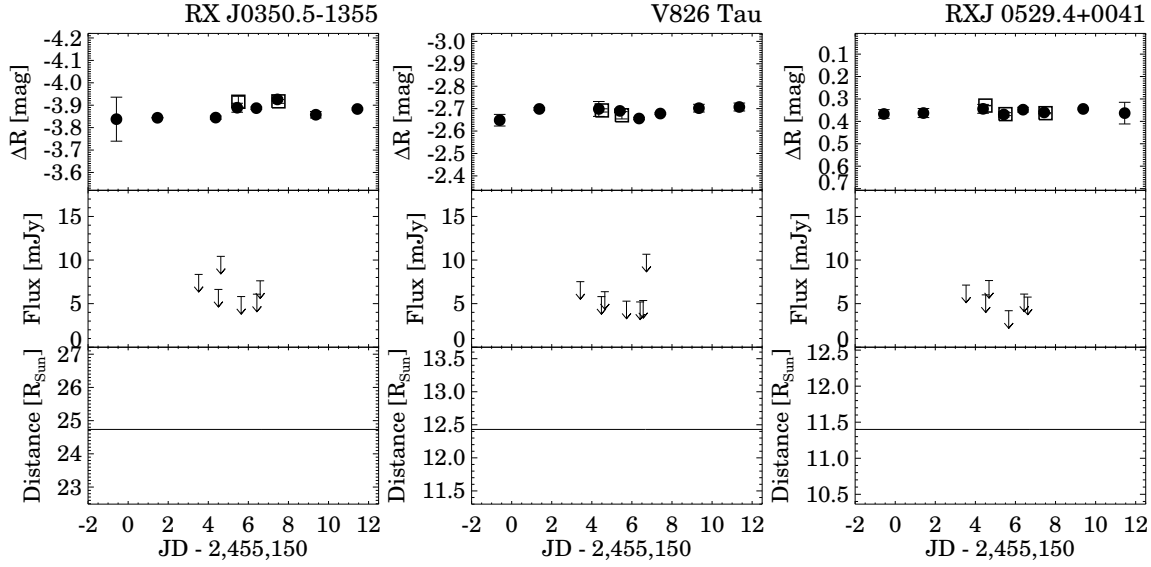

Figure 6.1 — (Continued)

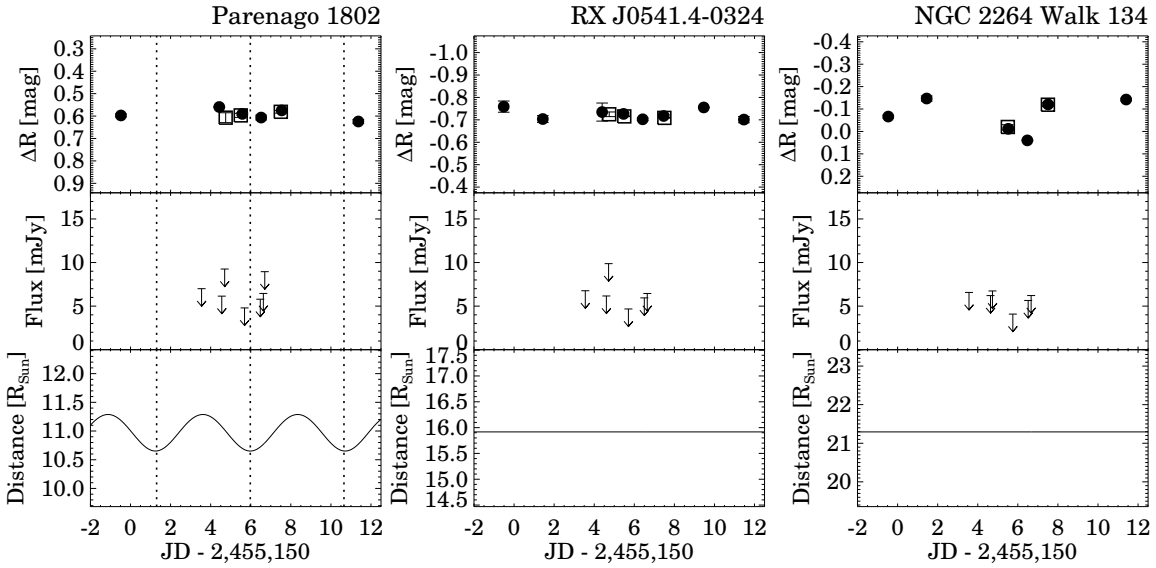

Figure 6.1 — (Continued)

source for which a potentially significant outer circumstellar disk may still be present. The other sources in our sample are more similar to V773 Tau A, with little to no remaining circumstellar material. We derive upper dust mass limits for the small-grain population of $\leq 3.0\times10^{-5}\,M_{\odot}$ ($0.003\,M_{\odot}$ for the total gas plus dust mass) for the sources in Taurus and $\leq 2.5\times10^{-4}\,M_{\odot}$ ($0.025\,M_{\odot}$ for the total gas plus dust mass) for the sources in Orion, on average. To make these dust mass estimates, we used the basic millimeter flux–mass relation of Dutrey et al. (1996) and take $\kappa_{\nu} = 0.02$ g cm^{-2} and $T_{\rm dust} = 45$ K. These upper limits are consistent with the optical–near infrared SEDs for these sources, which are usually fit well by a single-temperature stellar photosphere in the available literature.

The fact that 10 out of 12 of our sources are WTTS is largely a selection effect, due to the orbital parameters being easier to determine when stellar photospheric lines are not obscured by circumstellar material. In reality, the multiplicity ratio for CTTSs and WTTSs in Taurus is essentially identical (Kohler & Leinert 1998). Interestingly, WTTSs tend to dominate the X-ray sky in Taurus (Neuhaeuser et al. 1995; Güdel et al. 2007), suggesting that they are more magnetically active. If WTTSs are also more likely to experience the most powerful magnetic outbursts, our survey failed to detect an example of such an event.

Instead, it is the CTTS UZ Tau that exhibits millimeter variability. We detected UZ Tau at a level of 38–105σ over the course of our monitoring program, with its 1.25 mm flux varying between 107 and 199 mJy in a period of less than 4 days, a clear indication of a significant contribution of non-thermal emission processes. The millimeter light curve in Figure 6.1 shows two peaks: one at around periastron, and another one about two days later, with a deep minimum in-between the two maxima. Since UZ Tau is composed of two binaries, the telescope was always centered on the spectroscopic binary UZ Tau E, but UZ Tau W, at a distance of 3.8″, also had a contribution to the measured flux. As discussed later, we can assume that UZ Tau W is not brighter than UZ Tau E, and that its millimeter flux is constant in time, thus we attribute the observed variability to UZ Tau E. To rule out any instrumental artifacts (due to severe winds during the observing run), we re-checked the pointing, which we found to be good to within 2″ during all seven UZ Tau observations. Therefore, the absolute flux calibration for UZ Tau is precise to within 15%, which is better than the reported value for the entire sample. To produce a factor of 2 *decrease* in the flux—since a mispointing can only reduce the measured flux—the pointing error would have to be 5″, which is clearly not the case. Moreover, the highest fluxes we observed are higher

than values reported elsewhere, which cannot be created by mispointing. Thus, we take the flux changes reported here and in Figure 6.1 to be real.

6.4 Discussion

6.4.1 Event Statistics

Our goal was to understand the proliferation of millimeter flare events and variability within the context of a model for colliding magnetospheres, a phenomenon that on the surface appears fairly regular, is well described by a simple geometric model for overlapping fields, and has a relatively clear combination of parameters (e and $d_{\rm min}$) that are predicted to lead to powerful reconnection events visible at millimeter wavelengths. The idea is that the two stars at apoastron possess strong independent magnetospheres, but near periastron, the fields are more inclined to merge, or at least stretch or compress in the presence of one another, leading to reconnection events. This interaction radius is typically estimated to be $5\,R_\star$ based on a dipole magnetic topology and inner disk truncation models. However, in a binary system with a dynamically cleared inner disk and reduced magnetic braking of the stellar rotation from star-disk field lines, the fields may become stronger and extend further outwards. In our subsample of high-eccentricity candidate systems, we observed 1/6 sources to be active in the millimeter; and 0/6 sources for the circular orbits. This brings the number of documented millimeter-variable binaries to 3 (or 21%) of the combined 14-source sample, and includes V773 Tau A, DQ Tau, and now UZ Tau E (see Section 6.4.2).

We begin our analysis with the high-eccentricity sources. To proceed, we must make use of several derived quantities from the DQ Tau study to establish some detection constraints by generalizing all flares due to interbinary, large-scale magnetospheric collision events (Chapter 5, Salter et al. 2010). The borrowed properties include: the flare duration ($\sim$30 hours), peak brightness (100–500 mJy at 3 mm), occurrence ($\sim$2 events per orbital period), and decay time ($\sim$6.5 hours). All of our sources were observed approximately twice per night over a 4-day period, with a maximum average gap in the sampling of 16 hours. For DQ Tau, a typical event is estimated to maintain a flux $>$2 times quiescence for $\sim$75% of a flare (or $\sim$23 hours for the largest outbursts), meaning that our two high-eccentricity sources located in Taurus (140-160 pc away) were reasonably well sampled. However, for the four sources located in Orion (440-470 pc), at a distance 3 times further away where the flux density falls off as D^{-2}, our detection limit is reduced by a factor 9, meaning that a large flare may have only been detectable for about 5-6 hours. In these systems, flares might have been missed by the sparse sampling. This effect might explain the non-detection toward Parenago 2494, which is remarkably similar, in terms of orbital parameters, to UZ Tau E.

For the circular binaries, statistics are more difficult to discern since the phenomenon is based on chance collisions of extended coronal structures. Stars that are more magnetically active are likely, in theory, to exhibit statistically more common events, but this requires a large sample and an uninterrupted, long-duration monitoring program. If, instead, we consider the once-a-week statistical occurrence of giant X-ray outbursts (assuming these are magnetically driven), then having monitored the circular sources for half a week, we might have expected half of (all) the sources to have flared; instead, we detected no flares toward the circular binaries. Again, distance effects and sampling may have affected the five most distant ($>$ 400 pc) sources.

Our study highlights the challenges of establishing a statistically significant sample of well-parameterized spectroscopic binaries and carrying out sufficient monitoring of the sample. In Section 6.4.3, we discuss the systems on a source-by-source basis and we are able to attribute many system and stellar properties to our non-detection statistics, including: the sensitivity of our observations (which is a combination of a flare's flux density, the source distance, and our 3σ detection threshold), binary separation, orbital eccentricity, duration of the flare, spectral peak wavelength of the synchrotron emission, stellar magnetic field

strength and activity levels (also a function of spectral type), magnetosphere topology, and flare decay time (a function of field strength and separation distance). These factors may act to reduce our detection statistics, but not the actual rate of occurrence.

In the combined 14-source sample, it is the 3 most extremely eccentric, close-separation binaries that seem to experience very powerful magnetic events. Therefore, while a well-defined subclass of millimeter-flaring binaries may be taking shape, we also cannot exclude the detected flares as a potentially rare phenomenon amongst high eccentricity binaries.

6.4.2 UZ Tau

UZ Tau is a hierarchical quadruple system consisting of two binary systems UZ Tau E and UZ Tau W. The E component is a spectroscopic binary with an orbital period of 19.1 days (Mathieu et al. 1996), and at an angular separation of 3.8″ is the W component, which is itself a 0.34″ binary (Simon et al. 1995; Prato et al. 2002, and references therein). For the primary component of UZ Tau E, Jensen et al. (2007) give a spectral type of M1 and a photometric radius of $1.9\,R_{\odot}$. The UZ Tau E system is a CTTS system with ongoing accretion and clear infrared excess, indicating that warm material can be found close to the stars (see e.g. Furlan et al. 2006).

The Millimeter Picture

At millimeter wavelengths, Simon & Guilloteau (1992) observed UZ Tau with the IRAM PdBI in continuum at 2.7 mm and found that the resolved E and W components had equal fluxes of 13 ± 1 mJy. Later, Dutrey et al. (1996) observed the system again with the IRAM PdBI at the same wavelengh, only to report that the E component had a flux of 25.5 ± 1.6 mJy, this time about 3 times brighter than the W component, which measured a more consistent 8 ± 2 mJy. These contrasting observations suggest that the E component is highly variable, whereas W is more or less constant. We note that in both papers, data obtained at different orbital phases of the E component were combined to obtain one single flux value.

In our own survey, the UZ Tau source flux varied between 107 and 199 mJy, over a period of 4 days, and between orbital phases of -0.07 and 0.09. Although the IRAM 30 m telescope was centered on UZ Tau E, we did not completely resolve the system, therefore the W component had some contribution to these values ($\approx$ 70% of its flux may be included in the beam). Thus, we conclude that UZ Tau E varied between approximately 87 and 179 mJy at 1.25 mm. In comparison, previous 1.3 mm resolved fluxes from Jensen et al. (1996) and Isella et al. (2009) are respectively: 137 ± 28 mJy and 126 ± 12 mJy for UZ Tau E, and 32 ± 9 mJy and 30 ± 8 mJy for UZ Tau W. The sum of these are roughly centered between our most extreme values. These 1.3 mm flux values are very similar given the earlier 2.7 mm variability observed and the 13-year gap in time.

If we quickly compare these multi-wavelength fluxes for UZ Tau W, then for an average $F_{1.3\mathrm{mm}} \approx 31$ mJy and $F_{2.7\mathrm{mm}} \approx 10.5$ mJy, we find a millimeter spectral slope of $\alpha \approx 1.5$, which is consistent with an optically thin circumstellar (or circumbinary) disk. Performing a similar analysis on UZ Tau E, with $F_{1.3\mathrm{mm}} \approx 131.5$ mJy and a $F_{2.7\mathrm{mm}} \approx 20$ mJy, we derive an $\alpha \approx 2.6$, which is steeper but not unreasonable. We remark that our minimum $F_{1.25\mathrm{mm}}$ of 107 mJy (or $\approx$ 87 mJy without the W component) gives an $\alpha \approx 1.9$ that is also consistent with an optically thin disk, as well as the apparent dust evolutionary state of its neighboring W component, which likely formed at the same time and in the same local environment. Of course, due to the different geometry and system parameters, they might have evolved differently. In the end, what is most apparent, is how UZ Tau E seems to be characterized more often than not by excess non-thermal flux. Given the observations to date, our minimum UZ Tau E observation of 87 mJy represents our best measurement for the true quiescent thermal dust emission at 1.25 mm.

The example of UZ Tau E shows that large variations in millimeter brightness do occur, but they may

have many explanations. UZ Tau E was perhaps the most promising binary in the initial list because of its many shared traits with fellow spectroscopic binary DQ Tau. This includes of course the highest eccentricity in the sample and a close periastron approach, but also bipolar outflows and episodic accretion bursts from its own circumbinary disk (Basri et al. 1997; Jensen et al. 2007; Hirth et al. 1997). In the following paragraphs, we shall attempt to analyze the UZ Tau E data within the context of the DQ Tau model for colliding magnetospheres to see if this scenario might plausibly explain the active millimeter light curve.

In such a scenario, the apparent double-brightening present in the UZ Tau E millimeter light curve must represent two sequential events occurring two days apart. Salter et al. (2010, Chapter 5) also captured a secondary brightening toward DQ Tau within an estimated 15 hours of the first. In fact, there the authors predict a minimum of two events per periastron encounter in a scenario for colliding magnetospheres, corresponding to first the joining, and then the separation, of the two magnetospheres; a phenomenon that their restricted monitoring window was unable to test fully. In this work, covering a period of 4 days (or an observing window 6 times broader), we find it reasonable that the first break might occur more suddenly and closer to periastron, while the timing of the second event is likely to occur at a much larger separation distance as the magnetospheres slowly stretch and pinch off (see Figure 8 in Chapter 5, Salter et al. 2010). This would then result in an asymmetry of events around periastron. The UZ Tau E data show exactly this, where the first event occurs around the predicted periastron, and the second event seems to peak two days after periastron.

The two brightenings toward UZ Tau E possess similar recorded maximum fluxes, unlike the sequential events captured toward DQ Tau where the secondary is less bright. However, our sparse sampling means that in all likelihood we have missed the true maxima. In the second, third, and fourth data points represent a single, smooth decay, the duration of the first brightening appears comparable to those characteristic of DQ Tau ($\sim$30 hours). The second event is much more abrupt, with the last two data points being separated by only 4 hours, during which the source flux dropped by 73 mJy. The first peak observed toward UZ Tau occurs when the E component stars are separated by $\sim 22\,R_{\odot}$, and the second peak occurs when they are at a distance of $\sim 27\,R_{\odot}$. If reconnection occurs halfway between the stars in both cases, equivalent to stellar heights of $5.8\,R_{\star}$ and $7.1 R_{\star}$, then the synchrotron decay profiles should possess a factor of 2.5 difference in decay times, with the e-folding time for the first event approximately 4.3 hours and for the second event about 10.6 hours (see the analysis of Massi et al. 2006). The sampling of our data is too coarse to verify this.

The Optical Picture

Jensen et al. (2007) obtained BVRI photometry of UZ Tau E between 2003 and 2006, and claimed that its light curve is periodic on timescales equivalent to the orbital period. They interpreted these results as pulsed accretion from a circumbinary disk, according to the model by Artymowicz & Lubow (1996); an accretion model that, incidentally, was first tested observationally on data from DQ Tau (see Mathieu et al. 1997). In this model, the circumbinary disk is periodically perturbed by the eccentric binary components, causing the disk material to cross the gap between the disk and the stars and fall onto the stellar surfaces. The model predicts a smoothly varying accretion rate which can be more or less strongly peaked at periastron depending on the orbital parameters of the binary, and fits well the light curve presented in Jensen et al. (2007). They note, however, that the significant scatter in the light curves indicate that pulsed accretion does not occur during every binary orbit. Based on arguments concerning the amplitude and timescale of the variability, Jensen et al. (2007) discarded the possibility of rotational modulation due to stellar spots.

Our optical light curves obtained during the time of the millimeter observations indicate two peaks: one at periastron and the other about 3 days later. The peak-to-peak amplitude is 1.19, 0.96, and 0.57 mag

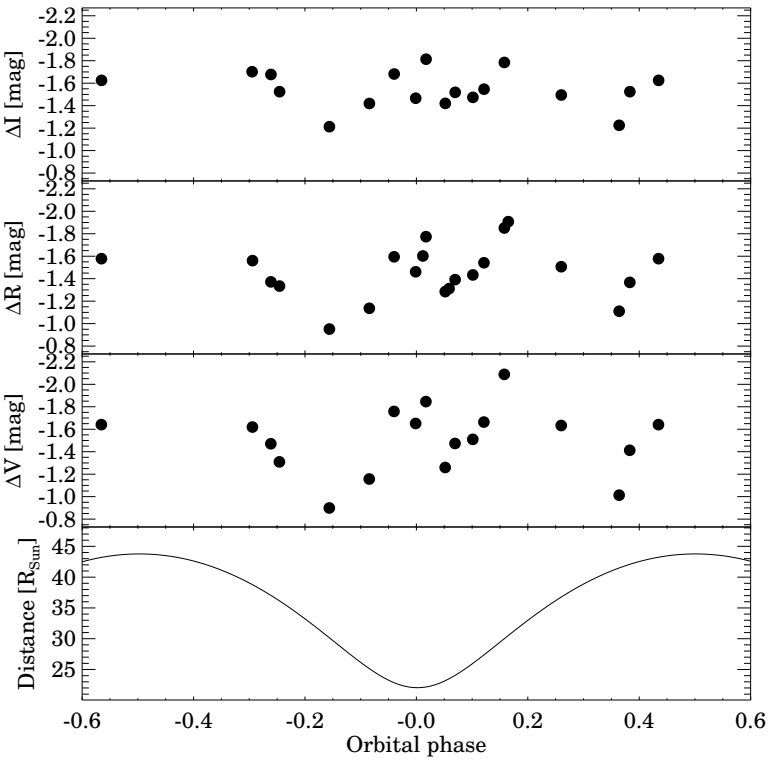

Figure 6.2 — Phase-folded optical light curves of UZ Tau E, and the separation of the binary components. A peak at an orbital phase of 0.00 and another one at 0.15 are clearly visible in the light curves, but the source was not completely quiescent even far from periastron.

in the V-, R-, and I-band, respectively indicating an amplitude decreasing with increasing wavelength. Additional optical observations obtained during the previous periastron show a very similar double-peaked light curve shape, suggesting that—at least for two adjacent periastrons—the optical light curve is periodic. Figure 6.2 shows the light curves folded with the orbital period of 19.131 days, clearly showing the two peaks: one at around 0.00 orbital phase, and another one at around 0.15. Although the light curves are not very well sampled far from periastron, it is evident that the source was not quiescent even when the binary components were far from each other.

Our results indicate that apart from varying accretion rate, a secondary contribution to the brightness changes can also be considered. The similar shape of the millimeter and the optical light curves suggest the possibility that optical flux changes may also be fueled by strong magnetic activity.

6.4.3 Other Sources

In the following paragraphs, we briefly discuss our results for the rest of the binaries within the context of the available literature data and our current analysis of the proliferation of powerful star-star magnetic reconnection events.

EK Cep is an eclipsing binary consisting of an A1.5V primary and a G5Vp secondary, with radii of 1.58 and 1.31 $R_{\odot}$, respectively (Torres et al. 2010). While the primary is already in the main-sequence phase, the secondary is still a PMS star (Marques et al. 2004). When referencing published photometry and the AKARI/IRC mid-IR all-sky survey (Ishihara et al. 2010), we found no evidence for infrared ex-

cess emission that is typically associated with ongoing accretion or warm inner circumstellar dust. Photometric observations by Antonyuk & Rostopchina (2009) indicate that, outside of the eclipse, no trends are noticeable in the light curves, although the scatter of data points does exceed their photometric uncertainty (± 0.04 mag). Antonyuk & Rostopchina (2009) detected variable polarization, which they attribute to surface magnetic activity of the secondary component. Our optical photometry shows that EK Cep was constant within our measurement uncertainties (± 0.02 mag), and the source was not detected during our millimeter observations. Our millimeter non-detection offers an upper limit of $M_{\rm disk} \leq 0.003\,M_{\odot}$ for the amount of material in the cold outer disk, if we use the basic flux-mass relation of Dutrey et al. (1996). EK Cep appears to be a fairly quiescent source from optical to millimeter wavelengths, and absent of very powerful star-star magnetic interactions throughout an entire orbital period.

RX J0530.7−0434 is a WTTS binary consisting of two identical, K2-K3 type stars with photometric radii of $3.40\,R_{\odot}$ (Covino et al. 2001; Marilli et al. 2007). Optical photometry by Covino et al. (2001) revealed photometric variations with a periodicity of 13.5 days (cf. the orbital period of 40.57 days). They interpret these results by supposing that the periodicity of the light curve is the rotation period (which is assumed to be similar for the two binary components), indicating non-synchronous rotation. Marilli et al. (2007) give a V-band amplitude of 0.22 mag and a rotational period of 12.9 days. We found no evidence in the literature for infrared excess to indicate the presence of warm circumstellar material. Our optical light curve shows slight variations with amplitudes of 0.12, 0.10, and 0.08 mag in V-, R-, and I-band, respectively, with the observed peaks approximately 5 days before and 3 days after periastron. The source was not detected during our millimeter observations, giving an upper limit of $M_{\rm disk} \leq 0.024\,M_{\odot}$ on the disk mass.

Parenago 1540 is a WTTS binary consisting of a K3V primary and a K5V secondary with no evident infrared excess (Marschall & Mathieu 1988). Manset & Bastien (2002) detected photometric variations with a V-band amplitude of < 0.5 mag, as well as periodic variations in the polarization, which they attribute to the orbital motion and the fact that there is still enough dust in the environment of the binary to produce polarization, despite the lack of infrared excess. Favata et al. (2005) reported the detection of an X-ray flare from this source observed during the COUP survey of the Orion Nebula Cluster. Our optical light curve shows a gradual brightening before periastron, and a fading after periastron. The amplitude of the variability is very similar in all bands (0.19 mag in V, 0.18 mag in R, and 0.13 mag in I). The source was not detected during our millimeter observations ($M_{\rm disk} \leq 0.025\,M_{\odot}$).

Parenago 2494 is a WTTS binary, the primary being an K0IV/V star (Reipurth et al. 2002). (Reipurth et al. 2002) found that the star shows periodic variability in the V-band with an amplitude of 0.10 mag and a period of 5.77 days (cf. the orbital period of 19.48 days). They interpret these variations as the result of large stellar spots on the primary component (which is assumed to dominate the optical light curve). We found no evidence in the literature for infrared excess. Our optical light curves also show variability with amplitudes of 0.12, 0.06, and 0.06 mag in V-, R-, and I-bands, respectively. Our coverage is not enough to do a period analysis, but the shape of the light curves is not inconsistent with a period of about 6 days. The source was not detected during our millimeter observations. Other than the absence of a significant circumstellar dust reservoir ($M_{\rm disk} \leq 0.028\,M_{\odot}$), Parenago 2494 possesses extremely similar orbital parameters to UZ Tau E. Located at a distance 3 times further away, a similar outburst as the one observed towards UZ Tau E would appear 9 times weaker, and just a few times the noise level.

GG Ori is a PMS eclipsing binary consisting of two nearly identical B9.5-type stars with radii of 1.852 and $1.830\,R_{\odot}$ (Torres et al. 2000). B- and V-band light curves by Torres et al. (2000) display a scatter that

is significantly larger than the photometric errors, thus intrinsic variability of one or both components is suspected. We found no evidence in the literature for infrared excess to indicate warm material close to the stars. Our optical observations show that GG Ori was constant within the measurement uncertainties outside of the primary eclipse recorded on the night of 20/21 November 2009, shortly before periastron. The source was not detected at all during our millimeter observations ($M_{\rm disk} \leq 0.023\,M_{\odot}$). We do remark how an eclipse that lasts longer than the flare event itself is likely to completely obscure it, assuming the trapped electron population lies within the eclipsing plane. In the case of GG Ori, at a distance 3 times further than our outbursts in Taurus, the detection window is also shortened as it is for Parenago 2494. Moreover, B-type stars are reported to be less magnetically active than later spectral types (their magnetic fields are below a few hundred G, and their X-ray emission is not due to magnetospheric reconnections but shocks in the stellar wind, Damiani et al. 1994; Hubrig et al. 2009).

RX J0350.5−1355 is a WTTS binary consisting of a K0-K1 primary and a K1-K2 secondary (Covino et al. 2001). Covino et al. (2001) and Marilli et al. (2007) found modulations in the optical light curve with a periodicity close to the orbital period. They attribute the 0.2 mag amplitude photometric variability to rotational modulation due to stellar spots, suggesting that the rotational and the orbital period is synchronized. They also note that the spectral lines of the primary indicate faster rotation and strong magnetic activity. We found no evidence in the literature for infrared excess. Our optical observations show variations with amplitudes of 0.08, 0.09, and 0.12 mag in V-, R-, and I-band, respectively. Our coverage is not enough to do a period analysis, but the shape of the light curves are not inconsistent with a period of about 9 days. The source was not detected during our millimeter observations, which cover an entire orbital period ($M_{\rm disk} \leq 0.030\,M_{\odot}$). If the primary is magnetically active, then the reconnection events may not be powerful enough or frequent enough to be detected in the millimeter.

V826 Tau is a WTTS binary consisting of two very similar K7V-type stars with radii of $1.44\,R_{\odot}$ (Reipurth et al. 1990). Reipurth et al. (1990) found sinusoidal light variations with an amplitude of 0.06 mag and a period that is slightly smaller than the orbital period. They attribute the variability to rotational modulation due to stellar spots. We found no evidence in the literature for infrared excess; Furlan et al. (2006) classifies it as a Class III (diskless) source. Using XMM-Newton observations, Giardino et al. (2006) detected significant X-ray variability with a factor of 2 amplitude on a five-day timescale, possibly related to coronal magnetic activity. Our light curves show slight variations with amplitudes of 0.05, 0.07, and 0.04 mag in V-, R-, and I-band, respectively. The source was not detected during our millimeter observations ($M_{\rm disk} \leq 0.003\,M_{\odot}$), which cover 1.5 orbital periods.

RX J0529.4+0041 is a WTTS triple system, consisting of RX J0529.4+0041 A, an eclipsing spectroscopic binary, and RX J0529.4+0041 B, a single star at a projected distance of 1.3″ (Covino et al. 2004). The eclipsing binary consists of a K1V-type primary and a K7-M0 secondary, with radii of 1.44 and $1.35\,R_{\odot}$, respectively. Covino et al. (2000) reported B- and V-band brightness variations unrelated to the eclipses, possibly connected to rotational modulation due to stellar spots and other phenomena driven by magnetic activity. Covino et al. (2004) found that the out-of-eclipse JHK light curves of the source can be best fitted if stellar spots are included in their model. Marilli et al. (2007) also observed out-of-eclipse variations with a V-band amplitude of 0.1 mag. Our VRI light curves show that this source was constant within 0.03 mag in all three bands. A possible explanation is that the stars experienced a less active period and had no spots on their surface during our optical observing campaign. We found no evidence in the literature for infrared excess, and the source was undetected during our millimeter observations ($M_{\rm disk} \leq 0.011\,M_{\odot}$).

Parenago 1802 is a WTTS eclipsing binary consisting of two very similar M2-type stars with radii of 1.82 and 1.69 $R_\odot$ (Stassun et al. 2008). Cargile et al. (2008) observed 0.05 mag peak-to-peak variations in the out-of-eclipse I-band light curve, indicating intrinsic variability. They claim that these variations have both a periodic and a stochastic component, suggesting that spots and chromospheric activity may both be present in the system. Our light curves also show variability with amplitudes 0.06 and 0.05 mag in R- and I-band, respectively. Stassun et al. (2008) found weak evidence for infrared excess at $> 5\mu$m, indicating the presence of a circumbinary disk and/or a faint third component in the system. However, the source was not detected during our millimeter observations ($M_{\rm disk} \leq 0.022\,M_\odot$).

RX J0541.4−0324 is a WTTS binary consisting of a G8 primary and a K3 secondary (Covino et al. 2001), with photometric radii of 2.8 and 1.8 $R_\odot$, respectively. Marilli et al. (2007) observed rotational modulation in the V-band light curve with an amplitude of 0.1 mag and period of 5 days, equal to the orbital pediod, indicating a synchronous rotation. Our VRI light curves show slight variations with an amplitude of 0.06 mag in all three bands, not inconsistent with a 5-day period. We found no evidence in the literature for infrared excess. The source was not detected during our millimeter observations ($M_{\rm disk} \leq 0.024\,M_\odot$).

NGC 2264 Walk 134 is a PMS binary consisting of two similar G-type stars with radii of 3.2 $R_\odot$ (Padgett & Stapelfeldt 1994). Koch et al. (1994) reported V- and R-band variability with an amplitude of 0.35 mag, but found no periodicity in the light curves. They also found that the V brightness of the object is not correlated with the V−R color. Using Chandra observations, Ramírez et al. (2004) found that the source is variable in the X-ray, but found no periodicity in the data, and the variability was not flare-like either. Although its weak emission lines make it a WTTS, it has a near-IR excess that is more typical of CTTS (Padgett & Stapelfeldt 1994). Archival Spitzer IRS spectra also indicates significant infrared excess up to 30μm. Our optical light curves show peak-to-peak variations of 0.22, 0.19, and 0.18 mag in V-, R-, and I-band, respectively. The source appears redder when fainter. This binary was not detected during our millimeter observations ($M_{\rm disk} \leq 0.088\,M_\odot$).

6.5 Summary and Conclusions

Using the IRAM 30m telescope, we have conducted a monitoring program covering 4 consecutive nights to study the millimeter variability toward 12 PMS spectroscopic binaries mostly in the Taurus and Orion star-forming regions. Here we report that one source, the CTTS UZ Tau E, experiences significant millimeter flux variations ($F_{1.25\,\rm mm}$ ranges from 87 to 179 mJy) on daily timescales, a clear indication of non-thermal emission processes near periastron. The rest of the sample, consisting mainly of WTTS up to three times more distant, remain undetected in the continuum for the duration of the campaign, defining upper flux limits of 5–10 mJy at 1.25 mm (240 GHz).

The motivation for our survey follows the recent discoveries of recurring, bright (up to 27 times quiescent values or peaking at about 0.5 Jy) millimeter outbursts toward the T Tauri binaries V773 Tau A (Massi et al. 2008) and DQ Tau (Chapter 5, Salter et al. 2010). Attributed to synchrotron activity from interbinary interactions of large magnetic structures, the phenomenon toward V773 Tau A is described as chance collisions between extended coronal features, whereas it has been proposed that the geometry of the DQ Tau system alone (specifically a large e and small $d_{\rm min}$) results in global interactions between the two closed stellar magnetospheres near periastron (Mathieu et al. 1997; Basri et al. 1997). Therefore, our target list consisted of 6 close-separation binaries with circular orbits ($e \approx 0$) that may experience activity at any time (but apparently did not do so during our observing run), as well as 6 geometrically

favorable high-eccentricity systems with activity most likely to occur near periastron (where we detect two possible events toward the source UZ Tau E).

In our sample, no system geometry is quite as extreme as DQ Tau, although our detected source UZ Tau E comes closest. Therefore, a positive detection of (double-peaked) variability near periastron toward UZ Tau E lends strong support to a similar global interbinary interaction; but does not confirm it. Instead, this detection brings our total millimeter-variable source statistics to 3 (i.e. V773 Tau A, DQ Tau, and UZ Tau E) out of 14 observed sources, and means that we may need to consider that millimeter flares are not so uncommon. In addition, as we examine the other systems in much greater detail, it becomes clear why we might not have expected to see, or might have missed, evidence of flares in these systems. The most important factor seems to be the flux-distance inverse relation, which affects our detection limits and sampling coverage. The study itself was also limited by the number of close-separation binaries that have been both identified and well characterized.

UZ Tau E should certainly be considered for follow-up observations to help characterize the light curve profile, also on orbital timescales, and to assess potential contributions from strongly varying free-free emission processes. We must also strongly caution against the reliability of any disk model for UZ Tau E that is based on continuum flux measurements until the true quiescent flux level can be established. In the future, ALMA will allow better monitoring of these systems, leading to a more complete analysis of the proliferation of strong millimeter activity in low-mass PMS binary systems, as well as how much energy can be released during a millimeter outburst and the magnetic field regeneration timescales possible in systems known to experience recurring outbursts.

Acknowledgements

This article publishes observations made with the IAC-80 telescope, operated by the Instituto de Astrofísica de Canarias at the Teide Observatory (Spain), and with the Schmidt telescope at the Piszkéstető Mountain Station of the Konkoly Observatory (Hungary); we are grateful for the granted telescope time. We thank C. Zurita Espinosa for obtaining the IAC-80 data as part of a routine observing program. We are also grateful to B. Ocaña and J. Santiago for their help during the IRAM 30 m observations. The research of ÁK, DMS, and MRH is supported by the Nederlands Organization for Scientific Research (NWO). This work has benefitted from research funding from the European Community's Seventh Framework Programme.

Appendix A

A.1 Millimeter and Optical Data

Table A.1 — Millimeter photometry

JD−2,450,000	$F_{1.25mm}$ [mJy]	$\sigma_{1.25mm}$ [mJy]
EK Cep		
5152.91	0.04	2.48
5153.96	-6.31	2.30
5154.08	1.14	3.33
5155.13	-0.85	2.20
5155.89	-0.22	1.64
5156.05	-3.61	2.66
RX J0350.5−1355		
5153.02	-1.13	2.78
5154.00	0.47	2.21
5154.12	-0.86	3.47
5155.14	-1.21	1.94
5155.93	-1.82	2.03
5156.09	4.86	2.54
V826 Tau		
5152.93	-1.16	2.51
5153.98	0.46	1.94
5154.15	-2.02	2.12
5155.23	-3.84	1.76
5155.91	1.91	1.73
5156.06	1.20	1.79
5156.22	-2.82	3.56
UZ Tau		
5152.93	174.3	2.7
5153.99	181.9	2.0
5154.15	154.5	2.0
5155.24	107.4	2.0
5155.91	172.7	1.6
5156.07	198.7	2.0
5156.23	125.5	3.3
RX J0529.4+0041		
5153.04	-0.66	2.38
5154.02	-2.61	2.00
5154.18	-0.58	2.55
5155.16	-1.00	1.40
5155.93	-2.56	2.03
5156.11	-1.82	1.92
RX J0530.7−0434		
5153.04	2.74	2.51
5154.02	2.78	2.04

Table A.1 — continued.

JD−2,450,000	$F_{1.25\,mm}$ [mJy]	$\sigma_{1.25\,mm}$ [mJy]
5154.19	2.23	2.95
5155.17	0.81	1.49
5155.94	0.79	2.25
5156.12	-2.16	1.88
5156.19	3.67	2.92
Parenago 1540		
5153.04	-2.35	2.50
5154.03	-0.64	2.17
5154.19	9.87	2.94
5155.18	0.22	1.47
5155.95	1.45	2.20
5156.12	5.12	2.09
5156.20	2.65	2.97
Parenago 1802		
5153.05	0.07	2.33
5154.05	4.97	2.05
5154.20	4.11	3.08
5155.19	4.58	1.60
5155.98	1.06	1.93
5156.13	10.7	2.2
5156.20	11.1	3.0
Parenago 2494		
5153.05	3.86	2.30
5154.10	-0.06	2.13
5154.21	2.27	3.51
5155.20	0.71	1.62
5155.99	1.12	1.91
5156.14	1.42	2.23
5156.21	-5.40	3.26
RX J0541.4−0324		
5153.05	0.14	2.25
5154.11	-1.88	2.06
5154.22	0.84	3.29
5155.21	0.25	1.56
5156.00	1.19	1.98
5156.15	5.00	2.15
GG Ori		
5153.06	2.11	2.22
5154.11	-2.09	2.06
5154.22	-5.52	3.16
5155.21	-0.81	1.54
5156.00	-3.06	1.89
5156.15	-1.94	2.06
NGC 2264 Walk 134		
5153.06	-2.41	2.19

Table A.1 — continued.

JD−2,450,000	$F_{1.25mm}$ [mJy]	$\sigma_{1.25mm}$ [mJy]
5154.14	2.51	2.07
5154.23	-1.56	2.25
5155.25	3.18	1.36
5156.02	-0.99	1.88
5156.16	-2.00	2.07

Table A.2 — Comparison stars used in the optical photometry

Target	Comparison
EK Cep	2MASS J21402804+6940328
RX J0350.5−1355	2MASS J03501856−1354489
V826 Tau	2MASS J04320358+1806038
UZ Tau E	2MASS J04323023+2552413
RX J0529.4+0041	2MASS J05291738+0042581
RX J0530.7−0434	2MASS J05303150−0434536
Parenago 1540	2MASS J05343988−0526420
Parenago 1802	2MASS J05351235−0536403
Parenago 2494	2MASS J05370922−0606445
RX J0541.4−0324	2MASS J05412862−0326581
GG Ori	2MASS J05431553−0036546
NGC 2264 Walk 134	2MASS J06405783+0956299

Table A.3 — Optical photometry. The magnitudes are differential magnitudes with respect to the comparison stars in Table A.2. S is for the Konkoly Schmidt Telescope (Hungary) and I is for the Teide IAC-80 telescope (Spain).

JD−2,450,000	ΔV [mag]	ΔR [mag]	ΔI [mag]	Tel.
EK Cep				
5149.28		−4.22(4)	−3.91(3)	S
5151.27	−4.61(6)	−4.25(2)	−3.89(5)	S
5154.24	−4.56(11)	−4.23(13)	−3.91(13)	S
5155.35	−3.76(5)	−3.44(1)	−3.18(7)	S
5155.41		−4.26(4)		I
5156.34		−4.22(4)	−3.89(2)	S
5157.38	−4.62(6)	−4.22	−3.89(3)	S
5159.24	−4.61(4)	−4.21(2)	−3.90(7)	S
5161.26	−4.61(8)	−4.28	−3.96(5)	S
RX J0350.5−1355				
5149.42	−3.82(1)	−3.84(10)	−4.03(7)	S
5151.47	−3.75(11)	−3.84(1)	−3.88(28)	S
5154.37	−3.77(5)	−3.84(1)	−3.98(4)	S
5155.44	−3.81(1)	−3.89(2)	−4.00(1)	S
5155.50		−3.92(2)		I
5156.40	−3.80(1)	−3.89(1)	−3.99(2)	S

Table A.3 — continued.

JD−2,450,000	ΔV [mag]	ΔR [mag]	ΔI [mag]	Tel.
5157.45	−3.82(1)	−3.93(1)	−4.01(1)	S
5157.52		−3.92(1)		I
5159.37	−3.80(5)	−3.86(1)	−3.98(3)	S
5161.44	−3.76(6)	−3.88(1)	−3.91(6)	S
V826 Tau				
5149.40	−3.18(6)	−2.65(3)	−2.16(3)	S
5151.38	−3.21(4)	−2.70(1)	−2.15(1)	S
5154.35	−3.24(3)	−2.70(3)	−2.17(3)	S
5154.59		−2.69(1)		I
5155.40	−3.20(1)	−2.69(1)	−2.16(1)	S
5155.50		−2.67(2)		I
5156.36	−3.17(1)	−2.66(1)	−2.14(1)	S
5157.42	−3.20(1)	−2.68(1)	−2.16(1)	S
5159.35	−3.27(4)	−2.70(2)	−2.17(1)	S
5161.36	−3.25(8)	−2.71(2)	−2.16(3)	S
UZ Tau E				
5129.62	−1.57(1)	−1.51(1)	−1.65(1)	I
5130.55	−1.26(1)	−1.28(1)	−1.47(3)	I
5133.63	−1.11(1)	−1.09(1)	−1.37(3)	I
5134.48	−1.71(1)	−1.54(3)	−1.63(1)	I
5135.58	−1.80(1)	−1.72(7)	−1.76(1)	I
5136.58	−1.42(4)	−1.34(2)	−1.47(4)	I
5137.57	−1.61(1)	−1.49(1)	−1.50(3)	I
5142.58	−1.36(1)	−1.32(1)	−1.47(4)	I
5143.57	−1.59(1)	−1.53(1)	−1.57(1)	I
5149.38	−1.47(36)	−1.37(9)	−1.68(2)	S
5151.39	−0.90(5)	−0.95(2)	−1.21(3)	S
5154.36	−1.65(2)	−1.46(2)	−1.47(1)	S
5154.60		−1.55(1)		I
5155.37	−1.26(2)	−1.28(1)	−1.42(1)	S
5155.50		−1.26(1)		I
5156.32	−1.51(1)	−1.43(1)	−1.47(1)	S
5157.40	−2.09(3)	−1.85(1)	−1.78(1)	S
5157.54		−1.86(1)		I
5159.36	−1.63(7)	−1.51(2)	−1.49(1)	S
5161.34	−1.01(7)	−1.11(3)	−1.23(2)	S
UZ Tau W				
5129.62	−1.21(1)	−1.22(1)	−1.60(1)	I
5130.55	−1.17(1)	−1.21(1)	−1.56(1)	I
5133.63	−1.27(1)	−1.27(1)	−1.66(3)	I
5134.48	−1.27(6)	−1.24(2)	−1.59(3)	I
5135.58	−1.25(2)	−1.34(8)	−1.65(2)	I
5136.58	−1.30(5)	−1.32(3)	−1.70(2)	I
5137.57	−1.27(1)	−1.29(1)	−1.62(1)	I
5142.58	−1.19(1)	−1.22(1)	−1.60(3)	I

Table A.3 — continued.

JD−2,450,000	ΔV [mag]	ΔR [mag]	ΔI [mag]	Tel.
5143.57	−1.22(1)	−1.26(1)	−1.59(1)	I
5154.60		−1.16(1)		I
5155.50		−1.25(1)		I
5157.54		−1.17(1)		I
RX J0529.4+0041				
5149.44	0.64(2)	0.37(2)	0.12(2)	S
5151.41	0.65(3)	0.36(2)	0.10(1)	S
5154.38	0.62(2)	0.34(2)	0.09(1)	S
5154.61		0.33(1)		I
5155.42	0.64(1)	0.37(1)	0.10(1)	S
5155.51		0.37(1)		I
5156.38	0.62(1)	0.35(1)	0.09(1)	S
5157.43	0.64(1)	0.36(1)	0.11(1)	S
5157.54		0.36(1)		I
5159.38	0.61(1)	0.34(1)	0.08(1)	S
5161.45	0.63(1)	0.36(5)	0.10(1)	S
RX J0530.7−0434				
5149.45	−1.05(2)	−0.53(3)	0.10(2)	S
5151.42	−1.12(1)	−0.56(1)	0.07(1)	S
5154.41	−1.02(1)	−0.46(1)	0.12(1)	S
5154.62		−0.46(1)		I
5155.48	−1.00(1)	−0.46(1)	0.15(1)	S
5155.51		−0.46(1)		I
5156.44	−1.01(1)	−0.46(1)	0.14(1)	S
5157.48	−1.04(1)	−0.50(1)	0.11(1)	S
5157.54		−0.50(1)		I
5159.39	−1.06(1)	−0.51(1)	0.10(1)	S
5161.46	−1.03(1)	−0.50(1)	0.12(2)	S
Parenago 1540				
5149.51	-0.92(1)	−1.08(1)	−1.19(1)	S
5153.49	-1.04(7)	−1.13(1)		S
5154.44	-1.02(1)	−1.16(1)	−1.26(2)	S
5155.52		−1.15(1)		I
5155.60	-1.02(1)	−1.17(1)	−1.26(3)	S
5156.55	-1.06(1)	−1.20(1)	−1.29(1)	S
5157.56	-1.11(1)	−1.25(1)	−1.32(2)	S
5161.38	-1.08(1)	−1.19(1)	−1.30(5)	S
Parenago 1802				
5149.52		0.60(1)	−0.26(2)	S
5154.43		0.56(1)	−0.30(1)	S
5154.65		0.61(2)		I
5155.52		0.60(1)		I
5155.58		0.59(1)	−0.27(1)	S
5156.52		0.61(1)	−0.26(1)	S
5157.55		0.57(1)	−0.28(1)	S

Table A.3 — continued.

JD−2,450,000	ΔV [mag]	ΔR [mag]	ΔI [mag]	Tel.
5157.55		0.58(1)		I
5161.37		0.62(1)	−0.25(1)	S
Parenago 2494				
5149.50	−2.78(1)	−2.52(1)	−2.36(1)	S
5153.47	−2.70(2)	−2.49(1)	−2.34(1)	S
5154.42	−2.73(3)	−2.50(1)	−2.35(3)	S
5154.66		−2.54(1)		I
5155.50	−2.78(1)	−2.53(1)	−2.37(1)	S
5155.53		−2.52(1)		I
5156.46	−2.82(1)	−2.56(1)	−2.40(1)	S
5157.50	−2.77(2)	−2.53(2)	−2.39(1)	S
5157.56		−2.52(2)		I
5161.39	−2.79(2)	−2.52(2)	−2.39(4)	S
RX J0541.4−0324				
5149.49	−0.60(1)	−0.76(2)	−0.90(2)	S
5151.44	−0.55(1)	−0.70(2)	−0.84(1)	S
5154.40	−0.59(1)	−0.73(4)	−0.90(2)	S
5154.67		−0.72(1)		I
5155.46	−0.58(1)	−0.73(1)	−0.88(1)	S
5155.53		−0.72(1)		I
5156.42	−0.54(1)	−0.70(1)	−0.85(1)	S
5157.47	−0.57(1)	−0.72(1)	−0.86(1)	S
5157.56		−0.71(1)		I
5159.47	−0.60(1)	−0.76(1)	−0.88(1)	S
5161.47	−0.55(1)	−0.70(1)	−0.84(1)	S
GG Ori				
5151.48		−0.10(2)	−0.06(3)	S
5153.44	−0.31(1)	−0.13(2)	−0.05(1)	S
5154.67		−0.10(1)		I
5155.54		0.19(1)		I
5155.54	−0.03(3)	0.15(3)	0.22(2)	S
5156.49	−0.31(1)	−0.12(1)	−0.05(1)	S
5157.52	−0.30(1)	−0.11(1)	−0.05(1)	S
5157.55		−0.11(1)		I
5159.48	−0.29(1)	−0.10(1)	−0.01(1)	S
5161.42	−0.29(2)	−0.10(2)	−0.04(1)	S
NGC 2264 Walk 134				
5149.53	0.10(1)	−0.07(1)	−0.23(1)	S
5151.45	−0.01(1)	−0.15(1)	−0.31(1)	S
5155.52	0.15(1)	−0.01(1)	−0.19(1)	S
5155.54		−0.02(1)		I
5156.48	0.22(1)	0.04(1)	−0.13(1)	S
5157.51	0.04(1)	−0.12(1)	−0.28(1)	S
5157.51		−0.12(1)		I
5161.40	0.02(1)	−0.14(1)	−0.29(1)	S

Bibliography

Antonyuk, K. A. & Rostopchina, A. N. 2009, Astrophysics, 52, 103
Artymowicz, P. & Lubow, S. H. 1996, ApJ, 467, L77+
Basri, G., Johns-Krull, C. M., & Mathieu, R. D. 1997, AJ, 114, 781
Bastian, T. S., Benz, A. O., & Gary, D. E. 1998, ARA&A, 36, 131
Baxter, E. J., Covey, K. R., Muench, A. A., et al. 2009, AJ, 138, 963
Boden, A. F., Torres, G., Sargent, A. I., et al. 2007, ApJ, 670, 1214
Bower, G. C., Plambeck, R. L., Bolatto, A., et al. 2003, ApJ, 598, 1140
Cargile, P. A., Stassun, K. G., & Mathieu, R. D. 2008, ApJ, 674, 329
Choi, M., Tatematsu, K., Hamaguchi, K., & Lee, J. 2009, ApJ, 690, 1901
Covino, E., Catalano, S., Frasca, A., et al. 2000, A&A, 361, L49
Covino, E., Frasca, A., Alcalá, J. M., Paladino, R., & Sterzik, M. F. 2004, A&A, 427, 637
Covino, E., Melo, C., Alcalá, J. M., et al. 2001, A&A, 375, 130
Damiani, F., Micela, G., Sciortino, S., & Harnden, Jr., F. R. 1994, ApJ, 436, 807
Duquennoy, A. & Mayor, M. 1991, A&A, 248, 485
Dutrey, A., Guilloteau, S., Duvert, G., et al. 1996, A&A, 309, 493
Favata, F., Flaccomio, E., Reale, F., et al. 2005, ApJS, 160, 469
Feigelson, E., Townsley, L., Güdel, M., & Stassun, K. 2007, Protostars and Planets V, 313
Forbrich, J., Menten, K. M., & Reid, M. J. 2008, A&A, 477, 267
Forbrich, J., Preibisch, T., Menten, K. M., et al. 2007, A&A, 464, 1003
Furlan, E., Hartmann, L., Calvet, N., et al. 2006, ApJS, 165, 568
Furuya, R. S., Shinnaga, H., Nakanishi, K., Momose, M., & Saito, M. 2003, PASJ, 55, L83
Getman, K. V., Feigelson, E. D., Broos, P. S., Micela, G., & Garmire, G. P. 2008a, ApJ, 688, 418
Getman, K. V., Feigelson, E. D., Micela, G., et al. 2008b, ApJ, 688, 437
Getman, K. V., Flaccomio, E., Broos, P. S., et al. 2005, ApJS, 160, 319
Ghez, A. M., McCarthy, D. W., Patience, J. L., & Beck, T. L. 1997, ApJ, 481, 378
Giardino, G., Favata, F., Silva, B., et al. 2006, A&A, 453, 241
Gimenez, A. & Margrave, T. E. 1985, AJ, 90, 358
Güdel, M. 2002, ARA&A, 40, 217
Güdel, M., Briggs, K. R., Arzner, K., et al. 2007, A&A, 468, 353
Hirth, G. A., Mundt, R., & Solf, J. 1997, A&AS, 126, 437
Hubrig, S., Stelzer, B., Schöller, M., et al. 2009, A&A, 502, 283
Isella, A., Carpenter, J. M., & Sargent, A. I. 2009, ApJ, 701, 260
Ishihara, D., Onaka, T., Kataza, H., et al. 2010, A&A, 514, A1+
Jensen, E. L. N., Dhital, S., Stassun, K. G., et al. 2007, AJ, 134, 241
Jensen, E. L. N., Koerner, D. W., & Mathieu, R. D. 1996, AJ, 111, 2431
Koch, R. H., Perry, P. M., & Kilambi, G. C. 1994, Information Bulletin on Variable Stars, 4032, 1
Kohler, R. & Leinert, C. 1998, A&A, 331, 977
Leinert, C., Zinnecker, H., Weitzel, N., et al. 1993, A&A, 278, 129
Luhman, K. L., Allen, P. R., Espaillat, C., Hartmann, L., & Calvet, N. 2010, ApJS, 186, 111
Manset, N. & Bastien, P. 2002, AJ, 124, 1089
Marilli, E., Frasca, A., Covino, E., et al. 2007, A&A, 463, 1081
Marques, J. P., Fernandes, J., & Monteiro, M. J. P. F. G. 2004, A&A, 422, 239
Marschall, L. A. & Mathieu, R. D. 1988, AJ, 96, 1956
Massi, M., Forbrich, J., Menten, K. M., et al. 2006, A&A, 453, 959
Massi, M., Menten, K., & Neidhöfer, J. 2002, A&A, 382, 152
Massi, M., Ros, E., Menten, K. M., et al. 2008, A&A, 480, 489

Mathieu, R. D., Martin, E. L., & Magazzu, A. 1996, in Bulletin of the American Astronomical Society, Vol. 28, Bulletin of the American Astronomical Society, 920–+
Mathieu, R. D., Stassun, K., Basri, G., et al. 1997, AJ, 113, 1841
Neuhaeuser, R., Sterzik, M. F., Schmitt, J. H. M. M., Wichmann, R., & Krautter, J. 1995, A&A, 297, 391
Neupert, W. M. 1968, ApJ, 153, L59+
Padgett, D. L. & Stapelfeldt, K. R. 1994, AJ, 107, 720
Prato, L., Simon, M., Mazeh, T., Zucker, S., & McLean, I. S. 2002, ApJ, 579, L99
Preibisch, T., Kim, Y., Favata, F., et al. 2005, ApJS, 160, 401
Ramírez, S. V., Rebull, L., Stauffer, J., et al. 2004, AJ, 127, 2659
Reipurth, B., Lindgren, H., Mayor, M., Mermilliod, J., & Cramer, N. 2002, AJ, 124, 2813
Reipurth, B., Lindgren, H., Nordstrom, B., & Mayor, M. 1990, A&A, 235, 197
Salter, D. M., Hogerheijde, M. R., & Blake, G. A. 2008, A&A, 492, L21
Salter, D. M., Kospal, K., Getman, K. V., Hogerheijde, M. R., & Blake, G. A. 2010, A&A, 123, in press
Simon, M., Ghez, A. M., Leinert, C., et al. 1995, ApJ, 443, 625
Simon, M. & Guilloteau, S. 1992, ApJ, 397, L47
Stassun, K. G., Mathieu, R. D., Cargile, P. A., et al. 2008, Nature, 453, 1079
Stassun, K. G., van den Berg, M., & Feigelson, E. 2007, ApJ, 660, 704
Stassun, K. G., van den Berg, M., Feigelson, E., & Flaccomio, E. 2006, ApJ, 649, 914
Stine, P. C., Feigelson, E. D., Andre, P., & Montmerle, T. 1988, AJ, 96, 1394
Testa, P. 2010, Proceedings of the National Academy of Science, 107, 7158
Torres, G., Andersen, J., & Giménez, A. 2010, A&A Rev., 18, 67
Torres, G., Lacy, C. H. S., Claret, A., & Sabby, J. A. 2000, AJ, 120, 3226
White, S. M., Pallavicini, R., & Kundu, M. R. 1992, A&A, 257, 557